Nonlinear Dynamics (2026) 114:501
https://doi.org/10.1007/s11071-026-12339-5

RESEARCH

Mode interaction in the presence of nonlinear friction: an asymptotic approach

Javier González-Monge[1] · Salvador Rodríguez-Blanco[2] · Carlos Martel[1]

Received: 19 September 2025 / Revised: 31 January 2026 / Accepted: 2 February 2026 / Published online: 5 April 2026

Abstract
We investigate the interaction between vibration modes coupled through nonlinear friction effects. Specifically, we consider the case where the mode shapes differ significantly, resulting in distinct friction cycles at contact interfaces. This scenario is common in mechanical systems such as bladed disks in turbomachinery, where friction, although localized to a few contact nodes, plays a key role in energy dissipation and induces strong nonlinearities in the system response. Standard time integration methods are often inefficient due to the numerical stiffness introduced by the small effect of friction. Harmonic Balance Methods offer a more efficient alternative and have recently been extended to handle nonlinear friction and two-frequency forcing. In this work, we present an alternative asymptotic approach based on a multiple scales expansion, yielding a reduced-order model that captures frictional effects on the slow timescale where they are developed. For the case of two simultaneously excited modes, the method leads to two coupled amplitude equations, where the influence of nonlinear friction is encoded through complex-valued functions that describe contact transitions and energy dissipation. The resulting model enables efficient parametric studies and analytical computation of nonlinear resonance curves. Validation on a lumped parameter system demonstrates good agreement with time-domain simulations and reveals that linear superposition significantly overestimates the system response.

Keywords Mode interaction · Nonlinear friction · Asymptotic methods · Multiple scales

1 Introduction

The accurate prediction of vibrations in mechanical structures is important across many engineering fields. Nonlinear effects, such as friction, complicate this analysis, invalidating the description of the response as a simple linear superposition of natural modes. In this work, we analyze nonlinear vibrations under simultaneous excitation of two different modes, each with a distinct modal frequency.

Finite Element Method (FEM) models are widely used in industry to compute structural dynamics. However, typical FEM models contain millions of degrees of freedom (DOFs), and the presence of nonlinear contact further increases computational cost. As a result, direct time integration becomes impractical for analyzing realistic models of engineering structures.

For this reason, Reduced Order Models (ROMs) are also used to provide a low-dimensional representation of a mechanical system while capturing the relevant dynamics. Common ROM methods include Craig-Bampton and Component-Mode Synthesis techniques [4, 6]. These approaches compute the modal shapes of different structural components and combine them to obtain a globally reduced description of the full assembly.

Nevertheless, these reduced systems still are subject to the nonlinearities of the problem. Dry friction, present at contact interfaces, is a highly nonlinear phenomenon. Although the relative displacements of the contacts are often small, their influence on the system response through energy dissipation by friction is very relevant. Even in the reduced problem, this effect increases numerical stiffness. Therefore, time integration becomes more difficult due to this stiffness and also requires solving the equations over many elastic cycles, as frictional dissipation develops over a long timescale. To

✉ Javier González-Monge
javier.gonzalez.monge@upm.es

1 Departamento de Matemática Aplicada a la Ingeniería Aeroespacial, Universidad Politécnica de Madrid, Madrid 28040, Spain

2 Departamento de Mecánica de Fluidos y Propulsión Aeroespacial, Universidad Politécnica de Madrid, Madrid 28040, Spain

address this issue, practical formulations of friction elements have been developed over the years [21, 26, 28] to model these nonlinearities and obtain results consistent with experiments.

Due to the limitations of time integration strategies for computing the periodic response of structures under harmonic loading, Harmonic Balance Methods (HBM) have been widely adopted [13]. These methods assume a periodic system response, and transform the differential equations describing the motion of the system to a set nonlinear algebraic equations, where the unknowns are the Fourier coefficients. The main difficulty lies in computing the nonlinear terms, which is typically handled using the Alternating-Frequency-Time (AFT) technique [5]. This approach evaluates the nonlinear forces in the time domain and then transforms them to the frequency domain. Using this framework, HBM has been successfully applied to systems with various nonlinear friction laws [14, 19, 24], obtaining the forced response functions.

Standard HBMs typically consider a fundamental frequency and its harmonics. In the presence of external forcing at multiple frequencies, these methods have been extended to account for a selected set of harmonics. By including geometric nonlinearities and two known excitation frequencies, HBM has been successfully used to compute the dynamic response of various systems [7, 11, 12, 25, 27]. For nonlinear friction laws, recent investigations have introduced different strategies to evaluate nonlinear forces in the frequency domain [2]. With a priori knowledge of the relevant harmonics, these extensions provide an effective tool to track two-frequency solutions. Additionally, by analyzing the stability of the response curves, bifurcation studies have been conducted [20].

Despite its widespread use, HBM has some limitations. By assuming a specific form of the solution, it only captures a particular response, which may be unstable and may fail to reveal the stable states of the system, especially when additional effects are present. For instance, in [9], it is shown that in the study of nonlinear interaction between flutter and forced response in a bladed-disk system, states where the flutter and forcing frequencies interact emerge from the synchronous solution with the forcing, and they could not be explored directly using HBM. Moreover, the method remains computationally expensive, as it requires solving a large nonlinear algebraic system for each value of the driving frequency.

For these reasons, asymptotic techniques have received attention in recent years, since they offer an alternative to accurately describe the full system dynamics within a specific regime of interest at a very reduced cost. More importantly, they highlight the relevant physical parameters that govern the response of the system, making them very practical during design stages of mechanical systems.

The asymptotic model uses multiple scales techniques [3] to derive an amplitude equation that captures the evolution of the system's slow envelope. These methods have been validated against ROM models [15, 16] and successfully applied to reproduce experimental results [22] in cyclic systems, where mode interaction was present but involved very similar mode shapes due to the flatness of the modal family. For nonlinear friction forces in the microslip regime [18], this approach enables the use of continuation techniques [1] to characterize the solution space through bifurcation diagrams. As a result, complex nonlinear dynamics can be captured without being restricted to periodic solutions [8, 9].

Recently, an extension of the asymptotic methodology was proposed to derive the amplitude equation directly from a high-fidelity FEM model including Coulomb friction [23], demonstrating the potential of these tools for application to realistic models. The nonlinear vibration of a structure near a resonance crossing was reduced to a one dimensional complex differential equation. The frictional contact behavior (including nonlinear transitions between stick, slip, and gap conditions) was encoded into a single complex friction function. The shape of this function provided physical insight into the contact transitions as a function of the excited mode's amplitude.

The goal of this paper is to extend the asymptotic methodology to study the simultaneous harmonic excitation of two different modes in the presence of nonlinear friction. The system response is expected to differ significantly from the linear superposition of modes, as nonlinear friction induces non-trivial interactions between them. We provide a systematic procedure to obtain amplitude equations that describe the evolution of both modal amplitudes.

The paper is structured as follows: first, we develop the asymptotic method for a generic structure derived from a FEM model, extending the analysis of the previously introduced single-mode asymptotic model. Then, the methodology is validated on a mass-spring model, representing mode interaction through a nonlinear friction element. The accuracy of the asymptotic model is assessed against time integration results, and the nonlinear interaction is compared to the linear superposition of modes.

2 Methodology

2.1 Problem description

The equations of motion describing the vibrations of a structure obtained from a FEM model are typically written as

$$\mathbf{M}\ddot{\mathbf{x}} + \mathbf{C}\dot{\mathbf{x}} + \mathbf{K}\mathbf{x} + \mathbf{G}(\mathbf{x}, \dot{\mathbf{x}}) = \mathbf{F}(t), \tag{1}$$

where $\mathbf{x}$ is the displacement vector, $\mathbf{M}$ is the mass matrix, $\mathbf{C}$ the linear damping matrix, and $\mathbf{K}$ the stiffness matrix. The nonlinear forces are contained in $\mathbf{G}(\mathbf{x}, \dot{\mathbf{x}})$, and $\mathbf{F}(t)$ represents the external forcing.

The nonlinear forces $\mathbf{G}(\mathbf{x}, \dot{\mathbf{x}})$ typically arise from dry friction at the contact interfaces of the structure. These forces act on a small subset of nodes, where the motion is usually much smaller than the displacements associated with the directly excited modes. In this regime, an asymptotic methodology can be applied to analyze the system's dynamic response, which consists of elastic harmonic oscillations modulated slowly by the nonlinear friction forces.

The interaction of modes through the nonlinearity introduced by friction is analyzed by applying an external forcing of the form

$$\mathbf{F}(t) = \mathbf{F}^A \cos(\omega_{f_A} t) + \mathbf{F}^B \cos(\omega_{f_B} t), \tag{2}$$

where ω_{f_A} and ω_{f_B} are the forcing frequencies, and $\mathbf{F}^A$, $\mathbf{F}^B$ are the corresponding forcing vectors. The case of interest considers both frequencies near two distinct resonances of the system, each associated with a different mode shape.

2.2 Asymptotic model

To derive the asymptotic description, we first partition the system in Eq. (1) into elastic and contact degrees of freedom (DOFs)

$$\begin{aligned} &\begin{pmatrix} \mathbf{M}_{ee} & \mathbf{M}_{ec} \\ \mathbf{M}_{ce} & \mathbf{M}_{cc} \end{pmatrix} \begin{pmatrix} \ddot{\mathbf{x}}_e \\ \ddot{\mathbf{x}}_c \end{pmatrix} + \begin{pmatrix} \mathbf{C}_{ee} & \mathbf{C}_{ec} \\ \mathbf{C}_{ce} & \mathbf{C}_{cc} \end{pmatrix} \begin{pmatrix} \dot{\mathbf{x}}_e \\ \dot{\mathbf{x}}_c \end{pmatrix} \\ &\quad + \begin{pmatrix} \mathbf{K}_{ee} & \mathbf{K}_{ec} \\ \mathbf{K}_{ce} & \mathbf{K}_{cc} \end{pmatrix} \begin{pmatrix} \mathbf{x}_e \\ \mathbf{x}_c \end{pmatrix} + \begin{pmatrix} 0 \\ \mathbf{g}(\mathbf{x}_c, \dot{\mathbf{x}}_c) \end{pmatrix} = \begin{pmatrix} \mathbf{f}(t) \\ 0 \end{pmatrix}, \end{aligned} \tag{3}$$

where $\mathbf{x}_e$ and $\mathbf{x}_c$ are the elastic and contact DOF displacements, respectively. The contact DOFs represent the relative motion at the contact interfaces, as the nonlinear forces are more naturally expressed in this form. In most practical cases, the number of elastic DOFs N_e is much larger than the number of contact DOFs N_c, i.e., $N_e \gg N_c$. The damping matrix is assumed to be small and proportional to the stiffness matrix, $\mathbf{C} = \beta \mathbf{K}$, and is included only for numerical stability. The dominant energy dissipation arises from the nonlinear contact forces.

In the asymptotic method [10], the displacements are expanded as

$$\begin{aligned} \mathbf{x}_e &= \mathbf{x}_e^{(0)} + \Psi \mathbf{x}_c^{(1)} + \mathbf{x}_e^{(1)} + \cdots, \\ \mathbf{x}_c &= \mathbf{x}_c^{(0)} + \mathbf{x}_c^{(1)} + \cdots, \end{aligned} \tag{4}$$

where $\Psi = -\mathbf{K}_{ee}^{-1}\mathbf{K}_{ec}$ represents the constraint modes. This expansion, which deviates from a straightforward asymptotic approach, is adopted because the influence of the contact displacements on the elastic field through this term is essential and is associated with motions close to rigid-body. Neglecting this effect leads to a systematic underestimation of the contact forces, even in linear analyses, as discussed in more detail in Chapter 4 of [10].

At zeroth order, the contacts are assumed to be fully stuck (i.e., bonded), so that

$$\mathbf{x}_c^{(0)} = \mathbf{0}, \tag{5}$$

as the motion at the contact interfaces is much smaller than that of the overall structure. The elastic displacements then follow from the first block of equations

$$\mathbf{M}_{ee}\ddot{\mathbf{x}}_e^{(0)} + \mathbf{K}_{ee}\mathbf{x}_e^{(0)} = 0, \tag{6}$$

where proportional damping and external forcing are assumed to be small and will appear at the subsequent order in the perturbation expansion. Equation (6) describes the free oscillations of the structure with bonded contacts. Its general solution takes the form

$$\mathbf{x}_e^{(0)} = \phi e^{i\omega t} \tag{7}$$

where the mode shapes ϕ and associated frequencies ω are obtained from the eigenvalue problem

$$(-\omega^2 \mathbf{M}_{ee} + \mathbf{K}_{ee})\phi = 0. \tag{8}$$

Two eigenpairs, (ω_A, ϕ_A) and (ω_B, ϕ_B), are selected to describe the two modes being forced in order to analyze their nonlinear interaction (without loss of generality, we assume $\omega_A < \omega_B$). These bonded modes are mass matrix normalized, i.e., $\phi_A^\top \mathbf{M}_{ee}\phi_A = 1$ and $\phi_B^\top \mathbf{M}_{ee}\phi_B = 1$. Additionally, an assumption of the asymptotic model is that the frequencies ω_A and ω_B are separated, with no neighboring modes in close proximity. The leading-order elastic displacements can then be written as

$$\mathbf{x}_e^{(0)} = A(\tau)e^{i\omega_A t}\phi_A + B(\tau)e^{i\omega_B t}\phi_B + \text{c.c.}, \tag{9}$$

where c.c. denotes the complex conjugate and the slow timescale τ has been introduced, which is much slower than the oscillation of the modes $\tau \gg 1/\omega_A, 1/\omega_B$.

The motion of the system consists of oscillations around two natural modes, modulated by the slowly varying envelopes $A(\tau)$ and $B(\tau)$. This follows a standard multiple scales methodology, where these envelopes capture the effects of higher-order terms, such as friction, linear damping, and external forcing. For a general review of perturbative techniques, see [3], and for the single-mode case, see [10, 23].

The next-order contribution, using the expansion in Eq. (4), and focusing on the equations associated with the contact DOFs, is governed by

$$(\mathbf{K}_{cc} - \mathbf{K}_{ce}\mathbf{K}_{ee}^{-1}\mathbf{K}_{ec})\mathbf{x}_c^{(1)} + \mathbf{g}(\mathbf{x}_c^{(1)}, \dot{\mathbf{x}}_c^{(1)})$$
$$= -\mathbf{K}_{ce}(2|A|\cos(\omega_A t + \varphi_A)\phi_A$$
$$+ 2|B|\cos(\omega_B t + \varphi_B)\phi_B), \tag{10}$$

where the inertial terms have been neglected. In oscillatory problems, stiffness terms are typically dominant over inertial terms, and both become comparable only near a natural frequency. In this contact problem, the frequencies ω_A and ω_B correspond to two natural frequencies of the elastic structure. However, since the contact stiffness (associated with $\mathbf{K}_{cc}$ and $\mathbf{M}_{cc}$) is much higher than the modal stiffness, inertial effects at the contact DOFs remain negligible compared to stiffness contributions (and this has also been verified numerically). Additionally, it is important to again highlight the significance of the term $\mathbf{K}_{ce}\mathbf{K}_{ee}^{-1}\mathbf{K}_{ec}$, which represents the coupling induced by the motion of the contact DOFs on the elastic field, which then feeds back into the contact interface. This reduction in effective stiffness is essential for accurately capturing the contact forces. This term is the one related to the constraint modes, since it can be identically rewritten as $\mathbf{K}_{ce}\mathbf{K}_{ee}^{-1}\mathbf{K}_{ec} = \Psi^\top \mathbf{K}_{ee}\Psi$, although we choose to write it in terms of the original FEM matrices for clarity in the implementation of the method.

This system of equations is analogous to the one obtained in [23] or [10] (Chapter 4) for a single mode, but here two distinct frequencies, amplitudes, and initial phases are considered. To solve it, we introduce two time variables

$$t_A = \omega_A t + \varphi_A, \quad t_B = \omega_B t + \varphi_B, \tag{11}$$

resulting in

$$(\mathbf{K}_{cc} - \mathbf{K}_{ce}\mathbf{K}_{ee}^{-1}\mathbf{K}_{ec})\mathbf{x}_c^{(1)} + \mathbf{g}(\mathbf{x}_c^{(1)}, \dot{\mathbf{x}}_c^{(1)})$$
$$= -\mathbf{K}_{ce}(2|A|\cos(t_A)\phi_A + 2|B|\cos(t_B)\phi_B). \tag{12}$$

The objective is to solve for the function $\mathbf{x}_c^{(1)}(t_A, t_B)$, which is 2π-periodic in both variables t_A and t_B, and depends on the modal amplitudes $|A|$ and $|B|$. As will be shown later, this step is central to the asymptotic process, as it enables the complex nonlinear dissipation behavior at the contacts to be encoded into two complex-valued functions. This approach extends what has previously been demonstrated for single-frequency reduced-order models [8, 9, 15, 16].

In addition, it is worth noting that this step bears some resemblance to the HBM approach for two-frequency forcing [2], but there is a fundamental difference between the two methods. In HBM, the contact displacements are known when evaluating the nonlinear forces. In contrast, in the asymptotic approach, the nonlinear friction forces are not evaluated using a technique such as AFT (Alternating Fourier Time); instead, they are included directly in the equilibrium and used to solve for the displacements in Eq. (12) for each fixed value of $|A|$ and $|B|$.

This process is more involved, as it requires solving an implicit partial differential equation

$$\mathbf{K}_{xx}\mathbf{x}_c^{(1)} + g\left(\mathbf{x}_c^{(1)}, \omega_A \frac{\partial \mathbf{x}_c^{(1)}}{\partial t_A} + \omega_B \frac{\partial \mathbf{x}_c^{(1)}}{\partial t_B}\right) = -\mathbf{K}_{ce}(2|A|\cos(t_A)\phi_A + 2|B|\cos(t_B)\phi_B), \tag{13}$$

where $\mathbf{K}_{xx} \equiv \mathbf{K}_{cc} - \mathbf{K}_{ce}\mathbf{K}_{ee}^{-1}\mathbf{K}_{ec}$, and the time derivative has been rewritten in terms of the two fast timescales as

$$\frac{\partial}{\partial t} \to \omega_A \frac{\partial}{\partial t_A} + \omega_B \frac{\partial}{\partial t_B}.$$

Nevertheless, unlike in HBM, this equation only needs to be solved once for various combinations of amplitudes $|A|$ and $|B|$. The $|A|$ and $|B|$ grid is generated by using some representative values of the maximum amplitude of the system, taken for example from the linear system, which constitutes an upper bound for the response when there is no friction. Then, as we show below, the nonlinear friction is then encoded into two complex functions, which can be used to compute the system response and perform parametric studies.

The general strategy to solve Eq. (13) is to start from a zero initial condition and compute the contact displacements until convergence is reached in both time scales, as illustrated in Fig. 1. Previous studies have shown that, for frictional contacts, convergence typically occurs after a few periods [17]. In this work, two periods were sufficient for the nonlinear friction effects to reach a periodic cycle in both time variables. The converged periodic solution is shown in blue, while the actual trajectories of the system are plotted in black. These trajectories evolve along a line with a slope equal to the ratio of the frequencies, reflecting the relationship between t_A and t_B.

The resulting solution, which is periodic in both variables, can be expressed as a two dimensional Fourier series

$$\mathbf{x}_c^{(1)}(t_A, t_B) = \sum_{n=-\infty}^{\infty} \sum_{m=-\infty}^{\infty} \mathbf{P}_{nm}(|A|, |B|) e^{int_A} e^{imt_B}, \tag{14}$$

where the Fourier coefficients $\mathbf{P}_{nm}(|A|, |B|)$ depend on the two modal amplitudes. The coefficients that capture the leading nonlinear effects are the first harmonics in each direction, namely $\mathbf{P}_{10}$ and $\mathbf{P}_{01}$, as will be discussed below. An interpolation of these coefficients over the amplitude space is performed to obtain continuous functions $\mathbf{P}_{10}(|A|, |B|)$ and $\mathbf{P}_{01}(|A|, |B|)$.

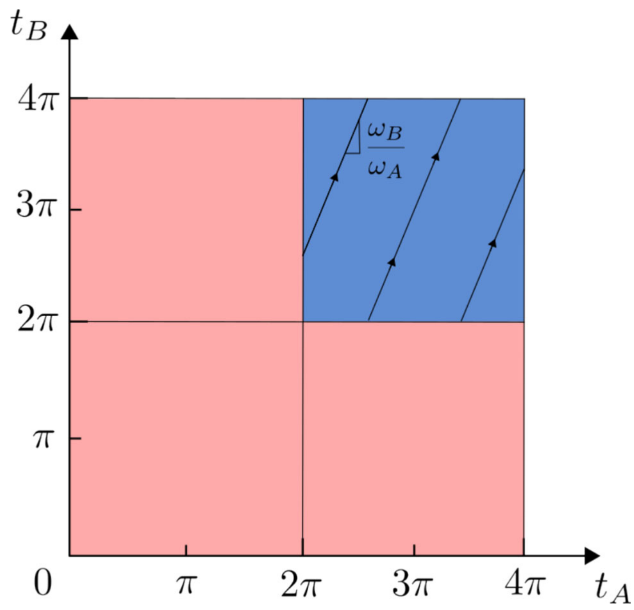

Fig. 1 Sketch of the periodic solution in two variables for the contact displacements

With the first correction of the contact displacement, coming back to the elastic equations we obtain

$$\mathbf{M}_{ee}\mathbf{x}_{e_{tt}}^{(1)} + \mathbf{K}_{ee}\mathbf{x}_{e}^{(1)} = -2\mathbf{M}_{ee}\mathbf{x}_{e_{t\tau}}^{(0)} + \mathbf{M}_{ee}\mathbf{K}_{ee}^{-1}\mathbf{K}_{ec}\mathbf{x}_{c_{tt}}^{(1)} - \beta\mathbf{K}_{ee}\mathbf{x}_{e_t}^{(0)} + \left(\frac{\mathbf{f}_A}{2}e^{i(\omega_A t + \Delta\omega_A \tau)} + \frac{\mathbf{f}_B}{2}e^{i(\omega_B t + \Delta\omega_B \tau)} + \text{c.c.}\right) \tag{15}$$

where the subscript t denotes differentiation with respect to the fast time, and τ with respect to the slow time. The inertial term $\mathbf{M}_{ec}\mathbf{x}_{c_{tt}}^{(1)}$ is neglected, as the effect of contact displacements on the full-stuck modes through the inertia is small. As mentioned before, the damping and forcing terms were assumed to be small parameters, and they are retained at this order in the expansion.

The forcing frequencies are written as small deviations from the natural frequencies, controlled by $\Delta\omega_A$ and $\Delta\omega_B$, since the goal of the asymptotic derivation is to describe the behavior near resonance crossings.

To compute the evolution equations for $A(\tau)$ and $B(\tau)$, a solvability condition is applied to the right-hand side (r.h.s) of Eq. (15) to ensure bounded solutions. Using the inner product

$$\langle \mathbf{f}, \mathbf{g} \rangle = \lim_{T\to\infty} \frac{1}{T}\int_0^T \bar{\mathbf{f}}^\top(t)\mathbf{g}(t)\mathrm{d}t, \tag{16}$$

the solvability conditions are given by

$$\langle \phi_A e^{i\omega_A t}, \text{R.H.S} \rangle = 0, \quad \langle \phi_B e^{i\omega_B t}, \text{R.H.S} \rangle = 0, \tag{17}$$

which enforce that the r.h.s is orthogonal to the nullspace of the self-adjoint operator on the left-hand side. These conditions yield the amplitude equations for $A(\tau)$ and $B(\tau)$ (details of their derivation are included in the Appendix A), which are given by

$$\frac{\mathrm{d}A}{\mathrm{d}\tau} + \xi_A A = -\frac{i}{2\omega_A}Q_A(|A|,|B|)A - \frac{i}{2\omega_A}f_A e^{i\Delta\omega_A\tau}, \tag{18}$$

$$\frac{\mathrm{d}B}{\mathrm{d}\tau} + \xi_B B = -\frac{i}{2\omega_B}Q_B(|A|,|B|)B - \frac{i}{2\omega_B}f_B e^{i\Delta\omega_B\tau}, \tag{19}$$

where $\xi_A = \beta\omega_A^2/2$ and $f_A = \phi_A^\top \mathbf{f}_A/2$, with analogous definitions for ξ_B and f_B. These two complex differential equations govern the evolution of the modal amplitudes $A(\tau)$ and $B(\tau)$ near their respective natural frequencies. The effect of nonlinear friction is encoded in the complex functions Q_A and Q_B, defined by the expressions

$$\begin{aligned} Q_A(|A|,|B|) &= -\frac{\phi_A^\top \mathbf{K}_{ec}\mathbf{P}_{10}(|A|,|B|)}{|A|}, \\ Q_B(|A|,|B|) &= -\frac{\phi_B^\top \mathbf{K}_{ec}\mathbf{P}_{01}(|A|,|B|)}{|B|}. \end{aligned} \tag{20}$$

These expressions correspond to the projection of the contact displacement solution in Eq. (14) onto the first harmonic in each direction. Only the first harmonics $\mathbf{P}_{10}$ and $\mathbf{P}_{01}$ appear, as they correspond to the resonant terms eliminated by the solvability condition.

In contrast to geometric nonlinearities, these functions are not the result of truncating a Taylor expansion at higher orders. Instead, they capture complex features of the contact behavior, including transitions and non-smooth effects, and must be retained in full within the asymptotic equations to preserve their influence at this order.

As previously mentioned, this asymptotic description is not limited to periodic solutions. It can also characterize more complex behavior when additional effects are included in the model, as demonstrated in [9] where quasi-periodic states where analyzed for the interaction of flutter and forced response in the presence of nonlinear friction.

Nevertheless, the system response at the forcing frequency is also a solution of the amplitude equations. This can be shown by assuming $A(\tau) = |A|e^{i\varphi_A}e^{i\Delta\omega_A\tau}$ and substituting into Eq. (18). (the derivation for $B(\tau) = |B|e^{i\varphi_B}e^{i\Delta\omega_B\tau}$ is analogous and omitted for brevity). To compute the resonance curve, we impose $\mathrm{d}|A|/\mathrm{d}t = 0$, yielding

$$\xi_A + i\Delta\omega_A = -\frac{i}{2\omega_A}Q_A(|A|,|B|) - \frac{i}{2\omega_A|A|}f_A e^{-i\varphi_A}. \tag{21}$$

Solving for the phase and amplitude leads to

$$\tan\varphi_A = \frac{\xi_A - \mathrm{Im}[Q_A]}{2\omega_A\Delta\omega_A + \mathrm{Re}[Q_A]}, \tag{22}$$

$$\Delta\omega_A = -\frac{\mathrm{Re}[Q_A]}{2\omega_A} \pm \sqrt{\left(\frac{f_A}{2|A|\omega_A}\right)^2 - \left(\frac{\mathrm{Im}[Q_A]}{2\omega_A} - \xi_A\right)^2}, \tag{23}$$

and similarly for mode B

$$\tan\varphi_B = \frac{\xi_B - \mathrm{Im}[Q_B]}{2\omega_B\Delta\omega_B + \mathrm{Re}[Q_B]}, \tag{24}$$

$$\Delta\omega_B = -\frac{\mathrm{Re}[Q_B]}{2\omega_B} \pm \sqrt{\left(\frac{f_B}{2|B|\omega_B}\right)^2 - \left(\frac{\mathrm{Im}[Q_B]}{2\omega_B} - \xi_B\right)^2}, \tag{25}$$

Equations (22) and (24) give the phase shift of the complex amplitudes, while Eqs. (23) and (25). implicitly define the amplitudes $|A|$ and $|B|$ for each value of the detuning parameters $\Delta\omega_A$ and $\Delta\omega_B$.

Therefore, the asymptotic procedure, once the nonlinear friction effects are characterized by the complex functions Q_A and Q_B, allows direct evaluation of the resonance curves $\Delta\omega_A(|A|, |B|)$ and $\Delta\omega_B(|A|, |B|)$ using simple analytical expressions. The main advantage of this approach is that the computational cost of evaluating the resonance curves for different forcing levels or damping values is very low, enabling efficient parametric studies.

In addition, if richer dynamics are present in the system (such as those induced by linear aerodynamic instabilities in turbomachinery) these solutions are still captured by the asymptotic equations and can be analyzed using continuation techniques, as demonstrated in [8, 9].

To summarize the asymptotic model, the procedure to derive the amplitude equations consists of the following steps:

1. Compute the linear bonded modes and natural frequencies (ω_A, ϕ_A) and (ω_B, ϕ_B).
2. Solve Eq. (13), perform a Fourier transform, and obtain the complex friction functions $Q_A(|A|, |B|)$ and $Q_B(|A|, |B|)$ using Eq. (20). This step involves selecting a grid of amplitude values $(|A|, |B|)$ and solving, for each pair, a system of equations of the size of the contact DOFs. The amplitude range can be estimated from the linear response of the system at resonance without friction, which provides an upper bound. The resulting data are then interpolated to evaluate $Q_A(|A|, |B|)$ and $Q_B(|A|, |B|)$ over the desired domain.
3. Once the friction functions have been computed, the analysis of mode interaction reduces to the asymptotic amplitude equations (18) and (19).
4. The resonance curves are obtained directly from Eqs. (23) and (25), reducing the nonlinear forced response problem to the evaluation of simple analytical expressions. This enables parametric studies with respect to system parameters such as f_A, f_B, and damping coefficients ξ_A and ξ_B.

Table 1 Values of the parameters used in the lumped model of Fig. 2.

m_1	m_2	m_c	k_1	k_2	k_{c_1}	k_{c_2}	k_p	μN	f_A	f_B
1.0	1.0	0.01	1.0	1.7^2	20	40	5	2.0	0.15	0.25

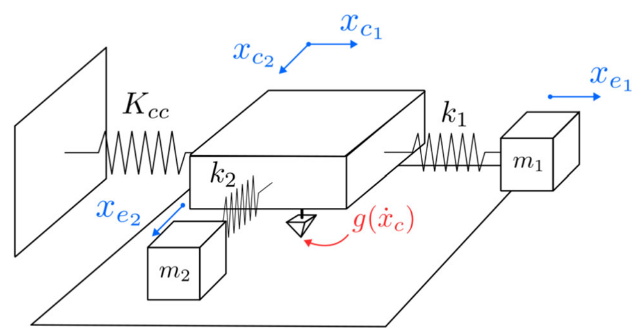

Fig. 2 Lumped model to study the interaction of modes. Two masses m_1 and m_2 that represent two modal displacements are interacting through a friction element

The most computationally intensive step in generating the asymptotic model is the evaluation of the nonlinear friction functions in step 2, which requires repeatedly solving a system of equations of the size of the contact DOFs. However, this step needs to be performed only once for a given nonlinear friction law, and in a mechanical structure the number of contact DOFs is typically much smaller than the total DOFs, since dry friction is present at the contact interfaces. After that, the remaining analysis is entirely based on the amplitude equations, which, as noted above, involves only the evaluation of simple analytical expressions, making this other part of the analysis computationally inexpensive. Moreover, one of the key advantages of the asymptotic model is that the influence of various system parameters on the response appears explicitly in the amplitude equations.

3 Results and discussion

The asymptotic procedure derived in the previous section is now applied to a specific case to investigate the effect of nonlinear friction under simultaneous excitation of different modes.

The model, shown in Fig. 2, consists of two masses, m_1 and m_2, representing the modal displacements of two distinct modes. These are coupled through a contact element that exerts nonlinear friction forces denoted by $g(\dot{x}_c)$.

Using the notation introduced in Eq. (3), the system matrices and forcing vector for this particular case are given by

$$\mathbf{M}_{ee} = \begin{pmatrix} m_1 & 0 \\ 0 & m_2 \end{pmatrix}, \quad \mathbf{M}_{ec} = \begin{pmatrix} 0 & 0 \\ 0 & 0 \end{pmatrix}, \quad \mathbf{M}_{cc} = \begin{pmatrix} m_c & 0 \\ 0 & m_c \end{pmatrix},$$
$$\mathbf{K}_{ee} = \begin{pmatrix} k_1 & 0 \\ 0 & k_2 \end{pmatrix}, \quad \mathbf{K}_{ec} = \begin{pmatrix} -k_1 & 0 \\ 0 & -k_2 \end{pmatrix}, \tag{26}$$
$$\mathbf{K}_{cc} = \begin{pmatrix} k_1 + k_{c_1} & k_p \\ k_p & k_2 + k_{c_2} \end{pmatrix},$$

and the forcing vector takes the form

$$\mathbf{f}(t) = \begin{pmatrix} f_A \sin(\omega_A t) \\ f_B \sin(\omega_B t) \end{pmatrix}. \tag{27}$$

The values of the system parameters are listed in Table 1. They are chosen to reflect the conditions assumed in the derivation of the asymptotic model: the contact motion is much smaller than the modal displacements, and its inertial effects are negligible. Additionally, the two modes are orthogonal and carry most of the system's mass. Under these conditions, the motion of the contact DOFs is expected to follow the quasi-static equilibrium described by Eq. (12), consistent with the assumptions of the asymptotic model. (This behavior of the contacts has been validated in realistic engineering models from turbomachinery, although involving a single mode, as shown in [10, 23]).

A smoothed Coulomb friction law is used for the contact forces, given by

$$g(\dot{x}_t) = \mu N \tanh\left(\frac{\dot{x}_t}{\alpha}\right), \tag{28}$$

where μ is the friction coefficient, N is the normal load, $\dot{x}_t$ is the relative sliding velocity at the contact interface, and α is the regularization parameter. For small values of α, this expression approaches the Coulomb limit, $g(\dot{x}_t) \sim \mu N \mathrm{sgn}(\dot{x}_t)$.

The contact force is modeled using two independent one dimensional friction elements, acting in the x_{c_1} and x_{c_2} directions. This modeling choice follows [28], which reported that the response obtained using two one dimensional elements closely approximates that of a full two dimensional friction element.

For this system, the fully stuck natural frequencies are $\omega_A = 1$ and $\omega_B = 1.7$, with the corresponding mode shapes $\phi_A = (1, 0)^\top$ and $\phi_B = (0, 1)^\top$. These were chosen to represent two distinct modes that interact through nonlinear friction.

The lumped system is first integrated in time using two forcing frequencies, each close to one of the modal frequencies, to examine the dynamics that the asymptotic description aims to capture. In these simulations, we consider both forcing vectors applied simultaneously, and the cases where only one forcing is applied at a time in each direction. This allows us to clearly distinguish the individual and coupled responses.

Figure 3a shows the modal displacement associated with the x_{e_1} DOF, where elastic oscillations with a slow envelope are observed–this is the typical behavior that the asymptotic procedure is designed to capture.

Figure 3b presents the evolution of the nonlinear contact force along x_{c_1} over five periods of the smallest frequency ω_A. The blue curve corresponds to the case where only the first mode ϕ_A is excited, resulting in a periodic response. In contrast, the red curve shows the response when both modes are excited simultaneously; in this case, the nonlinear force is no longer perfectly periodic.

Moreover, Figs. 3c and 3d show the evolution of the contact displacements over time, again comparing the case of single mode excitation to the case of modal interaction. The red line represents the contact motion when both modes are excited simultaneously. The blue and green lines correspond to the responses when only ϕ_A or ϕ_B is excited, respectively.

To verify that the modes interact through the nonlinear term (such that a linear superposition of the individual responses is not valid) the trajectory of the contact element is shown in Fig. 4. The trajectories corresponding to independent excitation of each mode are shown in blue and green; both are straight lines, indicating that the modes remain decoupled in those cases. However, when both modes are excited simultaneously, the trajectory (shown in red) deviates significantly from a straight line, clearly revealing a nonlinear interaction between the modes.

It is also useful to plot the friction cycles over several periods. Fig. 5 shows the friction cycle for the contact in the x_{c_1} direction over five periods. The blue curve corresponds to excitation only along the x_{e_1} direction. In this case, the friction cycle forms a stable rectangle, and the energy dissipated, given by the enclosed area, remains constant in time, as the response is purely periodic.

In contrast, the red curve represents the evolution of the friction cycle when both modes are active. The shape and position of the cycle continuously shift over time, highlighting the presence of nonlinear interaction between the modes through the frictional contact.

The asymptotic derivation from the previous section is now applied, where the key step was the quasi-static equilibrium given in Eq. (12). This equation enables the characterization of the nonlinear effects that appear in the amplitude equations. The remainder of the derivation involves straightforward projections along the relevant modal directions. For the friction law considered here, the quasi-static correction

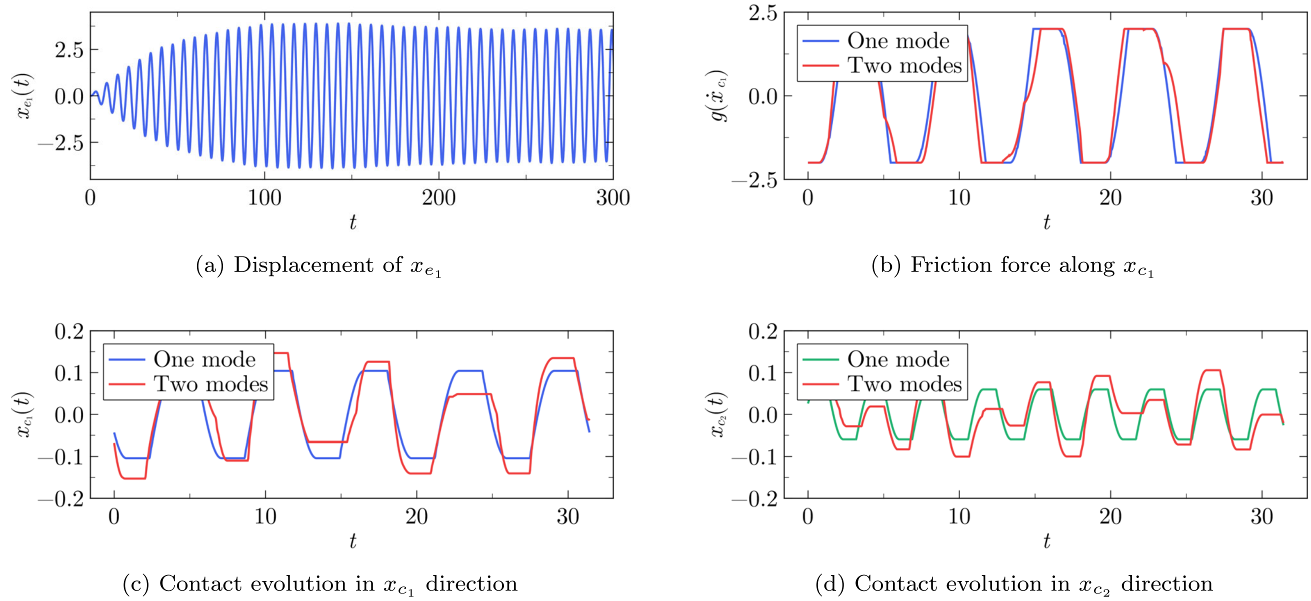

Fig. 3 Time integration of the lumped model with nonlinear friction

takes the form

$$(\mathbf{K}_{cc} - \mathbf{K}_{ce}\mathbf{K}_{ee}^{-1}\mathbf{K}_{ec})\mathbf{x}_c^{(1)} + \mu N \tanh(\dot{\mathbf{x}}_c^{(1)}/\alpha) = \\ -\mathbf{K}_{ce}(2|A|\cos(t_A)\phi_A + 2|B|\cos(t_B)\phi_B). \tag{29}$$

Recall that, by expanding the time derivative using the time variables t_A and t_B, the quasi-static correction can be written as an implicit partial differential equation in both variables

$$(\mathbf{K}_{cc} - \mathbf{K}_{ce}\mathbf{K}_{ee}^{-1}\mathbf{K}_{ec})\mathbf{x}_c^{(1)} \\ +\mu N \tanh\left(\frac{1}{\alpha}\left[\omega_A\frac{\partial \mathbf{x}_c^{(1)}}{\partial t_A} + \omega_B\frac{\partial \mathbf{x}_c^{(1)}}{\partial t_B}\right]\right) = \\ -\mathbf{K}_{ce}(2|A|\cos(t_A)\phi_A + 2|B|\cos(t_B)\phi_B). \tag{30}$$

To solve this system of equations, we discretize the time variables using $t_{A_n} = n\Delta t,\quad t_{B_m} = m\Delta t$, and denote the numerical solution of the PDE at the time instants (t_{A_n}, t_{B_m}) by $\mathbf{x}_{c_{nm}}^{(1)}$, yielding

$$(\mathbf{K}_{cc} - \mathbf{K}_{ce}\mathbf{K}_{ee}^{-1}\mathbf{K}_{ec})\mathbf{x}_{c_{nm}}^{(1)} \\ + \mu N \tanh\left(\frac{1}{\alpha}\left[\omega_A\frac{\mathbf{x}_{c_{nm}}^{(1)} - \mathbf{x}_{c_{n-1m}}^{(1)}}{\Delta t} + \omega_B\frac{\mathbf{x}_{c_{nm}}^{(1)} - \mathbf{x}_{c_{nm-1}}^{(1)}}{\Delta t}\right]\right) \\ = -\mathbf{K}_{ce}(2|A|\cos(n\Delta t)\phi_A + 2|B|\cos(m\Delta t)\phi_B), \tag{31}$$

which results in a nonlinear system of equations. Starting from the initial condition $\mathbf{x}_{c_{nm}}^{(1)} = \mathbf{0}$ for $n = 0$, $m = 0$, the two-dimensional periodic solution is obtained by solving over two periods in each timescale. The first period allows the frictional response to evolve, so that a periodic state is reached in the second cycle, as illustrated in Fig. 1.

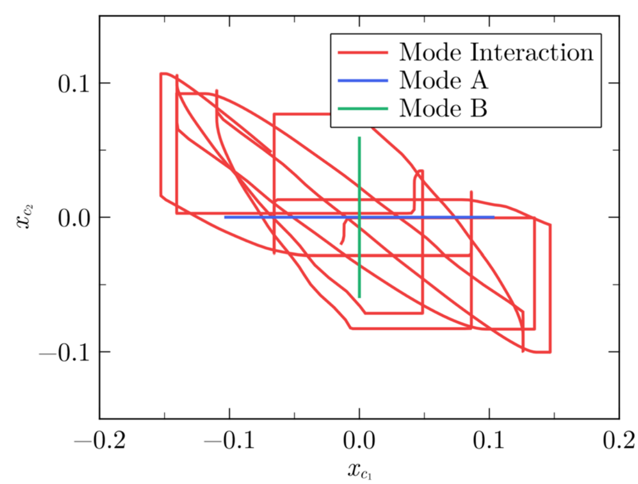

Fig. 4 Trajectory of the contact element of the lumped model: excitation with only ϕ_A (blue), only ϕ_B (green), and both modes interacting (red)

The described numerical procedure is carried out for the range of values $|A|, |B| \in [0, 3]$, using 50 points for each of the amplitudes. To illustrate this process, for the first contact, using $|A| = 1.3$ and $|B| = 1.5$, the resulting displacement as a function of both time variables is shown in Fig. 6. On the left, the displacements are plotted as a two-dimensional surface over a single period in each direction, after the friction effects have converged to a periodic state.

This solution is periodic in both directions and can therefore be visualized on a torus, as shown in Fig. 6(b). The torus is parametrized by two angles, each corresponding to one of the time scales, as highlighted in the figure. However, the system does not evolve arbitrarily over the torus surface, since

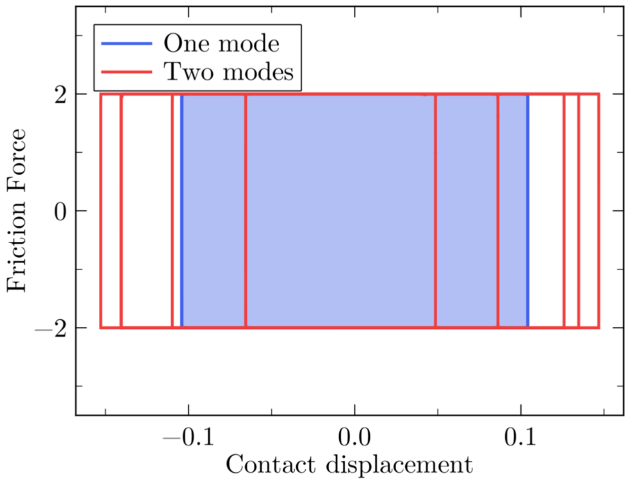

Fig. 5 Friction cycle for one mode (blue) and two modes (red)

the two time variables are related by

$$t_B = \frac{\omega_B}{\omega_A}(t_A - \varphi_A) + \varphi_B, \tag{32}$$

which defines a straight line in the (t_A, t_B) plane. Consequently, the actual system trajectory follows the black line shown on the torus, which will densely cover the surface if the ratio ω_B/ω_A is irrational (i.e., the frequencies are incommensurable).

Validations have been conducted to assess the accuracy of the asymptotic approach. First, the relative contributions of the terms in Eq. (29) were compared against results from full time-domain integration. In Fig. 7, the temporal evolution of the elastic and friction forces from Eq. (29) is shown. Their combined effect exhibits a nearly sinusoidal behavior, consistent with the r.h.s of the equation. For reference, the result from full time integration is plotted with a dashed line, showing excellent agreement, with only minor deviations near the peaks.

An additional comparison was performed with increased forcing amplitudes, specifically $f_A = 0.5$ and $f_B = 0.75$. The results, shown in Fig. 8, indicate that even at these higher forcing levels, the asymptotic solution closely matches the time integration results. Since one assumption in the asymptotic model is that the forcing amplitudes are small (of the same order as the damping), the errors increase with higher forcing levels, especially near the peak, but the results remain within the accuracy expected from the method.

In addition, the contact displacements were also examined. In the asymptotic formulation, these displacements are obtained by traversing the torus shown in Fig. 6, following the straight-line trajectory dictated by the slope in Eq. (32). The corresponding comparison is presented in Fig. 9, where subfigures (a) and (b) show the evolution of the two contact directions. In both cases, the response exhibits two dominant frequencies, and the asymptotic predictions show excellent agreement with the full time-domain solution.

The process is done for the range of values for $|A|$ and $|B|$ stated above, with the objective to characterize the complex friction functions $Q_A(|A|, |B|)$ and $Q_B(|A|, |B|)$ within the region of interest. These functions are computed from the first-order Fourier harmonics via the projection defined in Eq. (20), and are interpolated over the amplitudes range.

The resulting two-variable functions are plotted in Fig. 10, where the real and imaginary parts are displayed separately. Fig. 10a shows the real part of the complex friction function associated with mode A, i.e., Q_A. This component corresponds to the nonlinear frequency shift of the resonance.

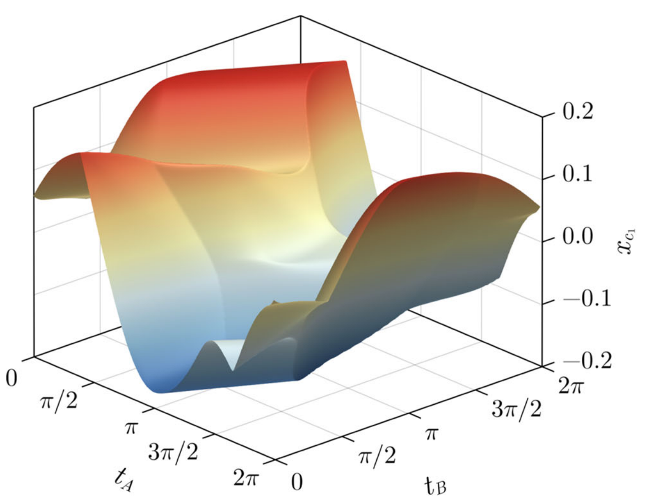

(a) Periodic surface of the x_{c_1} contact

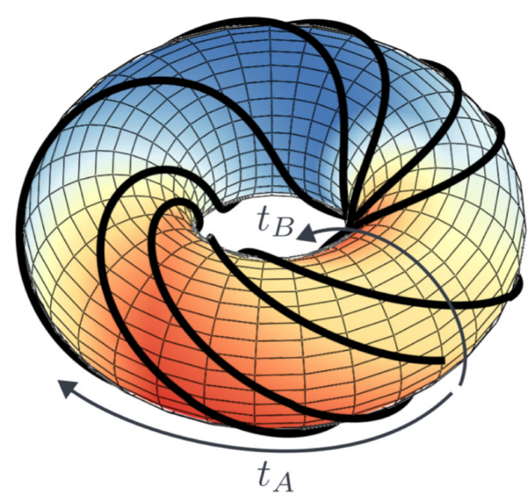

(b) Solution wrapped on a torus

Fig. 6 Periodic solution of the contact displacements in the two timescales corresponding to each mode. The black line on the torus highlights the quasiperiodic solution, which evolves along both timescales with a slope equal to the ratio of the natural frequencies

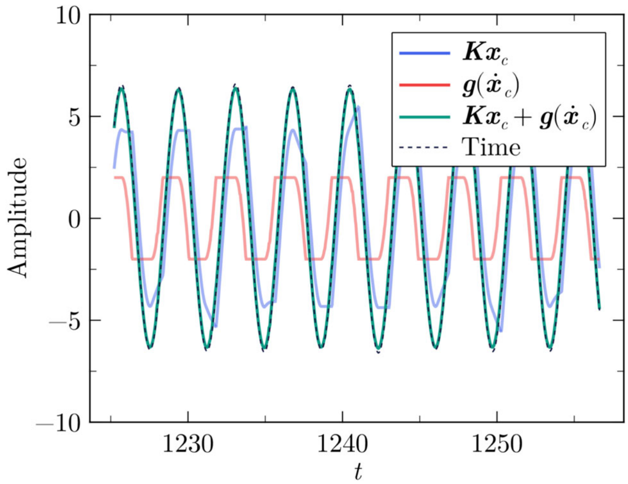

Fig. 7 Comparison of the different terms in the asymptotic equation against direct time integration results

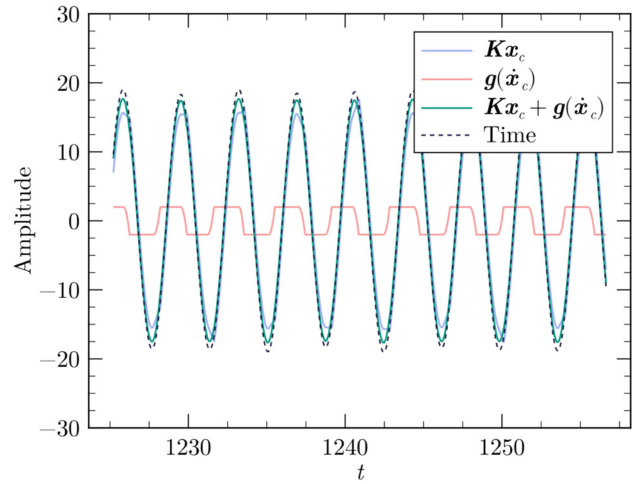

Fig. 8 Comparison of the different terms in the asymptotic equation against direct time integration results for an increased value of the forcings, $f_A = 0.5$, $f_B = 0.75$

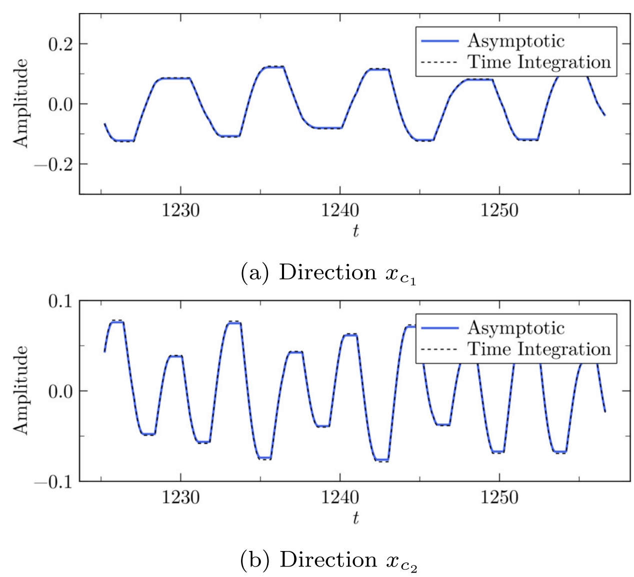

Fig. 9 Validation of the two-frequency solutions computed with the asymptotic process against direct time integration results

The plot clearly shows that increasing the amplitude $|B|$ significantly alters the frequency shift, producing a stronger deviation from the linear resonance compared to the case where $|B| = 0$.

Similarly, Fig. 10b shows the imaginary part of Q_A, representing the nonlinear damping introduced by Coulomb friction. The more negative this value, the greater the energy dissipation. As observed, the damping increases for nonzero values of $|B|$, though the surface is not strictly monotonic. This indicates the existence of certain amplitude combinations where the contact dissipates more energy, revealing a complex, nonlinear interaction between the modes.

Turning our attention to Q_B, the nonlinear frequency shift is also clearly influenced by the amplitude of mode A, as shown in Fig. 10c . Likewise, the imaginary part of Q_B, plotted in Fig. 10d , reveals increased damping levels for nonzero values of $|A|$.

Furthermore, both functions Q_A and Q_B exhibit negligible frequency shift and damping for small modal amplitudes. This behavior is expected, as the nonlinear friction is not active when the contact displacements remain below certain thresholds.

For clarity, Fig. 11 shows 2D slices of the complex friction functions to illustrate how the response evolves with different modal amplitudes. In particular, Figs. 11a and 11b highlight the influence of mode B on Q_A. When mode B becomes active, evident at $|B| = 0.5$ and $|B| = 1.0$, the frictional effects associated with mode A become present earlier, and the damping increases significantly. For example, at $|A| \sim 1.0$, the damping is substantially higher compared to the case when only mode A is excited.

A similar trend is observed in the real part of Q_A, which governs the nonlinear frequency shift. The presence of mode B produces a greater shift in the resonance peak, indicating stronger coupling between the modes through the friction interface.

The influence of mode A on the real and imaginary parts of Q_B is also analyzed in Figs. 11 (c) and (d), yielding results analogous to those discussed in the previous paragraph. As $|A|$ increases, both the nonlinear frequency shift and damping associated with mode B are significantly affected, further confirming the strong coupling introduced by friction.

In summary, at this stage of the asymptotic procedure, the complete effect of the nonlinear friction is encapsulated in the two complex functions Q_A and Q_B. These are the only nonlinear terms appearing in the amplitude equations, Eqs. (18) and (19). Consequently, once $Q_A(|A|, |B|)$ and $Q_B(|A|, |B|)$

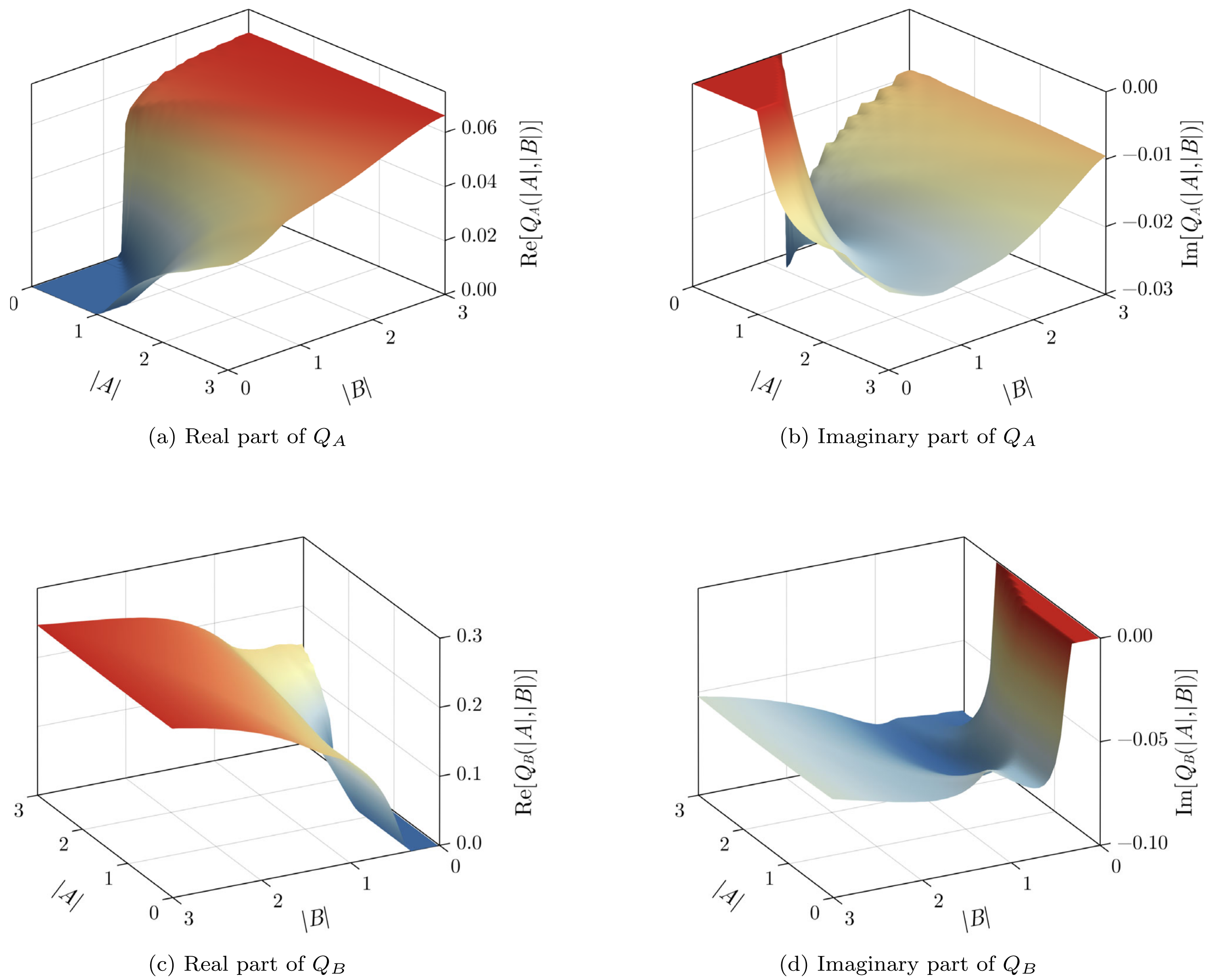

(a) Real part of Q_A

(b) Imaginary part of Q_A

(c) Real part of Q_B

(d) Imaginary part of Q_B

Fig. 10 Complex friction functions Q_A and Q_B

have been computed, the resonance curves can be obtained directly from simple evaluations of analytic expressions.

The resonance curves for the lumped system are now computed using the complex friction functions previously shown in Fig. 10, and by evaluating Eqs. (23) and (25).

These resonance curves are plotted in Fig. 12. The solution is traced over a range of forcing frequencies $\Delta\omega_A$ and $\Delta\omega_B$, corresponding to values near each modal resonance. To quantify the system's overall response when both modes are interacting, the vertical axis displays the quantity $\sqrt{|A|^2 + |B|^2}$, representing the maximum total displacement amplitude across time.

For a fixed value of $\Delta\omega_B$, a slice along $\Delta\omega_A$ corresponds to the resonance crossing associated with the first mode. The curve in blue, plotted for $\Delta\omega_B = -0.2$, which lies far from the resonance peak of mode B, recovers the response when only mode A is significantly excited. As shown, the system exhibits a typical softening behavior in the resonance region, induced by the nonlinear friction effects.

Conversely, by fixing $\Delta\omega_A = 0.2$, which is sufficiently far from the resonance of mode A, the green curve highlights the frequency response dominated by mode B. Although the resonance peak is lower compared to that of mode A, the amplitudes of both modes are of similar magnitude. This curve also reveals a nonlinear frequency response shape due to frictional effects.

Additional slices of the resonance curves are plotted in Fig. 12, showing how the response evolves as the system approaches both resonance frequencies simultaneously. These slices progress from the blue and green curves toward the red ones, which correspond to traversing each resonance while the other mode is near its peak response.

If the system response were governed solely by linear superposition, the shape of the blue curve (associated with mode A) would remain unchanged across all slices, simply

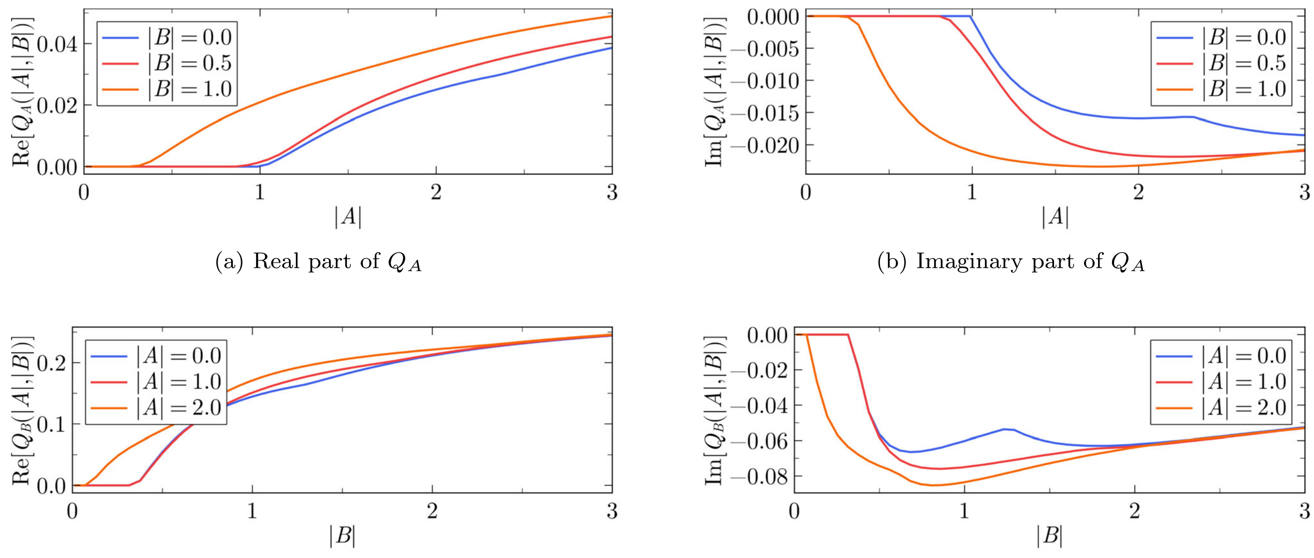

(a) Real part of Q_A (b) Imaginary part of Q_A

(c) Real part of Q_B (d) Imaginary part of Q_B

Fig. 11 Slices of the two dimensional complex friction functions Q_A and Q_B

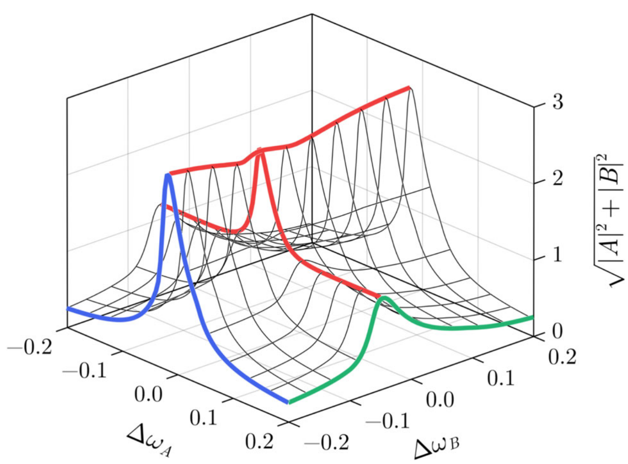

Fig. 12 Resonance curve at the resonance crossing with $\Delta\omega_A$ and $\Delta\omega_B$. The z-axis shows the maximum Euclidean norm of the displacements over time. The blue and green curves correspond to the resonances of modes A and B, respectively, while the red curve represents the interaction of both modes

shifting vertically by the amplitude of the mode B response. However, this is not observed. Instead, the red curves demonstrate that the resonance peak along $\Delta\omega_A$ is actually reduced compared to the case where mode A is excited in isolation.

This reduction is a direct result of increased nonlinear damping when both modes are simultaneously active, as previously illustrated in the complex friction functions Q_A and Q_B (see Fig. 11). The interaction between the modes through nonlinear friction fundamentally alters the energy dissipation and overall system dynamics.

To better illustrate the effect of nonlinear friction on modal interaction, a specific slice of the resonance surface corresponding to the resonance of both modes is shown in Fig. 13. On the left panel, the resonance curve across the first resonant frequency is presented.

In blue, the curve for $\Delta\omega_B = -0.2$ is shown, corresponding to a regime where mode A dominates the response. For comparison, the linear superposition of both modal responses is shown in black. This case assumes that mode B is at resonance, with $\Delta\omega_B = -0.046$, and simply adds the peak amplitudes from the individual responses. As expected from linear theory, the peak amplitude increases significantly–from approximately 2.5 to almost 4.

However, the actual nonlinear response of the system is plotted in red and results in a very different response. Despite both modes being near resonance, the peak amplitude remains similar to that of mode A excited alone. As the frequency moves away from the resonance of mode A, the amplitude asymptotically approaches the peak value of mode B.

This behavior highlights the non-trivial interaction caused by the nonlinear friction, which suppresses the overall amplitude due to increased damping, contradicting what would be predicted by a simple linear superposition of the modes.

A similar phenomenon is observed for mode B, as shown in Fig. 13(b). In this case, the green curve represents the response when mode B dominates the dynamics. For comparison, the linear superposition of both modes is plotted in black, obtained by simply adding the amplitude of the resonance peak of mode A to every point of mode B's response curve.

However, the actual system response, shown in red, deviates significantly from the linear prediction. Due to the nonlinear friction coupling, the damping of the system

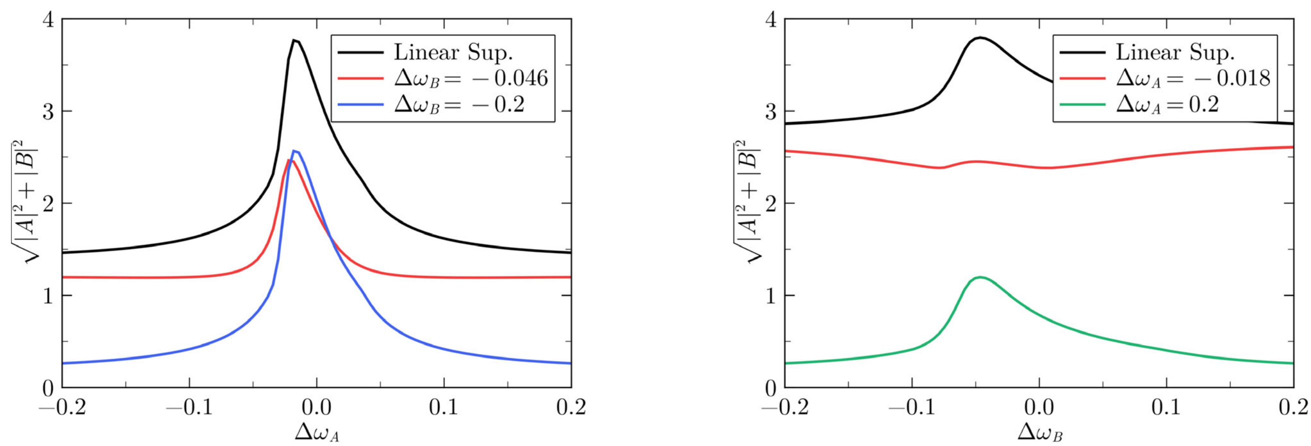

(a) Resonance crossing of ω_A

(b) Resonance crossing of ω_B

Fig. 13 Comparison of the resonance curves for both modes, including the effect of nonlinear frictional interaction and the simple linear superposition of both responses

increases, which leads to a reduced overall amplification. In fact, the amplitude at resonance is smaller than at nearby detuning values of $\Delta\omega_B$.

This counterintuitive behavior is explained by the enhanced dissipation from friction when both modes are simultaneously excited. As one moves away from the resonance in $\Delta\omega_B$, the influence of mode A becomes dominant again. Since mode A's individual resonance peak is higher than the coupled response at mode B's resonance, the system amplitude increases slightly–recovering the response that would occur without modal interaction.

4 Conclusions

This paper introduces a novel asymptotic modeling framework for analyzing mode interactions in the presence of nonlinear friction effects. Unlike traditional Harmonic Balance Methods (HBM), which rely on the assumption of periodicity with a fixed number of harmonics, the proposed asymptotic method captures the full dynamics of the system within a specified regime of interest, such as the steady-state response to resonant two-frequency forcing. The asymptotic methodology is based on a multiple-scales approach, exploiting a separation of timescales: one associated with the elastic oscillations at the system's natural frequencies, and a much slower one corresponding to the timescale on which friction effects become relevant. In addition to the dimensionality reduction, a key feature of asymptotic methods is that the resulting amplitude equations offer physical insight into the mechanisms governing the nonlinear behavior.

The method is suited for mechanical systems where contact occurs at a small subset of the total degrees of freedom, and where the relative motion at the contacts is small compared to the displacements along the excited mode shapes. Despite the small motion at the contact interface, the nonlinear friction forces can still have a significant influence on the overall response.

The asymptotic model reduces the mode interaction analysis to two amplitude equations, one for each mode, yielding a highly reduced-order model that retains the essential nonlinear dynamics of the full system. The resonance curves for each mode can then be efficiently computed by identifying periodic solutions of the amplitude equations, reducing the problem to the evaluation of simple analytical expressions. This enables rapid parametric studies that would be prohibitively costly using full time-domain simulations.

The characterization of nonlinear friction in the asymptotic model is achieved by solving a reduced system whose size is limited to the number of contact DOFs. This involves solving a periodic boundary value problem at the contact level only once; the remaining analysis is carried out entirely through the two amplitude equations. The influence of friction is then encoded in two complex-valued functions that depend on the amplitudes of the interacting modes. Analysis of these functions reveals that both nonlinear damping and frequency shift vary significantly when both modes are simultaneously excited.

The proposed methodology is validated on a representative lumped parameter model. Comparison with direct time integration shows excellent agreement, confirming the accuracy of the asymptotic approach. Notably, the resonance curves demonstrate that linear superposition fails to capture the true system behavior: when both modes are excited near their respective resonances, the increased nonlinear dissipation leads to a reduced peak amplitude, contrary to what a linear combination of the individual responses would suggest.

Since the asymptotic method developed here provides a low-dimensional and efficient framework for describing nonlinear mode interactions in mechanical structures where contact motion is small compared to the global modal displacements, future work will explore its applicability to more realistic cases, as well as to systems involving other types of nonlinearities.

Appendix A: Details of the asymptotic derivation

In this Appendix we provide additional details on the application of the solvability conditions

$$\langle \phi_A e^{i\omega_A t}, \text{R.H.S}\rangle = 0, \quad \langle \phi_B e^{i\omega_B t}, \text{R.H.S}\rangle = 0,$$

to the r.h.s of Eq. (15). We proceed by expanding each term separately and isolating the resonant contributions, as only those will appear in the amplitude equations. This follows from the orthogonality of the exponential functions

$$\frac{\omega}{2\pi}\int_0^{2\pi/\omega} e^{-in\omega t} e^{im\omega t}\,\mathrm{d}t = \delta_{nm},$$

where δ_{nm} is the Kronecker delta. Using Eq. (9), we first compute

$$-2\mathbf{M}_{ee}\mathbf{x}^{(0)}_{e_{t\tau}} = -2i\mathbf{M}_{ee}(\omega_A A_\tau e^{i\omega_A t}\phi_A + \omega_B B_\tau e^{i\omega_B t}\phi_B + \text{ c.c.}). \tag{33}$$

Since the bonded modes ϕ_A, ϕ_B are mass-normalized, the inner products yield

$$\begin{aligned}\langle \phi_A e^{i\omega_A t}, -2\mathbf{M}_{ee}\mathbf{x}^{(0)}_{e_{t\tau}}\rangle &= -\,2i\omega_A A_\tau,\\ \langle \phi_B e^{i\omega_B t}, -2\mathbf{M}_{ee}\mathbf{x}^{(0)}_{e_{t\tau}}\rangle &= -\,2i\omega_B B_\tau.\end{aligned} \tag{34}$$

Next, using Eq. (14), we evaluate

$$\begin{aligned}&\mathbf{M}_{ee}\mathbf{K}_{ee}^{-1}\mathbf{K}_{ec}\mathbf{x}^{(1)}_{c_{tt}}\\ &= \mathbf{M}_{ee}\mathbf{K}_{ee}^{-1}\mathbf{K}_{ec}(-\omega_A^2\mathbf{P}_{10}(|A|,|B|)e^{i\omega_A t+\varphi_A}\\ &\quad - \omega_B^2\mathbf{P}_{01}(|A|,|B|)e^{i\omega_B t+\varphi_B} + \text{c.c.} + \text{N.R.T.}),\end{aligned} \tag{35}$$

where N.R.T. denotes non-resonant terms, which vanish under the inner product. Noting that $A = |A|e^{i\varphi_A}$ and $B = |B|e^{i\varphi_B}$, we rewrite the previous expression as

$$\begin{aligned}&\mathbf{M}_{ee}\mathbf{K}_{ee}^{-1}\mathbf{K}_{ec}\mathbf{x}^{(1)}_{c_{tt}}\\ &= \mathbf{M}_{ee}\mathbf{K}_{ee}^{-1}\mathbf{K}_{ec}\Big(-\omega_A^2\frac{\mathbf{P}_{10}(|A|,|B|)}{|A|}Ae^{i\omega_A t}\\ &\quad -\omega_B^2\frac{\mathbf{P}_{01}(|A|,|B|)}{|B|}Be^{i\omega_B t} + \text{c.c.} + \text{N.R.T.}\Big).\end{aligned} \tag{36}$$

Taking the inner products gives

$$\begin{aligned}\langle \phi_A e^{i\omega_A t}, \mathbf{M}_{ee}\mathbf{K}_{ee}^{-1}\mathbf{K}_{ec}\mathbf{x}^{(1)}_{c_{tt}}\rangle &= -\frac{\phi_A^\top\mathbf{K}_{ec}\mathbf{P}_{10}(|A|,|B|)}{|A|}A,\\ \langle \phi_B e^{i\omega_B t}, \mathbf{M}_{ee}\mathbf{K}_{ee}^{-1}\mathbf{K}_{ec}\mathbf{x}^{(1)}_{c_{tt}}\rangle &= -\frac{\phi_B^\top\mathbf{K}_{ec}\mathbf{P}_{01}(|A|,|B|)}{|B|}B,\end{aligned} \tag{37}$$

where the identity $\phi_A^\top\mathbf{M}_{ee}\mathbf{K}_{ee}^{-1} = \frac{1}{\omega_A^2}\phi_A^\top$, has been used, which follows directly from the eigenvalue problem and the symmetry of the matrices. Using the definition of the complex friction functions in Eq. (20), we obtain

$$\begin{aligned}\langle \phi_A e^{i\omega_A t}, \mathbf{M}_{ee}\mathbf{K}_{ee}^{-1}\mathbf{K}_{ec}\mathbf{x}^{(1)}_{c_{tt}}\rangle &= Q_A(|A|,|B|)A,\\ \langle \phi_B e^{i\omega_B t}, \mathbf{M}_{ee}\mathbf{K}_{ee}^{-1}\mathbf{K}_{ec}\mathbf{x}^{(1)}_{c_{tt}}\rangle &= Q_B(|A|,|B|)B.\end{aligned} \tag{38}$$

For the linear damping term, using Eq. (9), we compute

$$\begin{aligned}-\beta\mathbf{K}_{ee}\mathbf{x}^{(0)}_{e_t} &= -\beta\mathbf{K}_{ee}(i\omega_A Ae^{i\omega_A t}\phi_A\\ &+ i\omega_B Be^{i\omega_B t}\phi_B + \text{ c.c.}),\end{aligned} \tag{39}$$

whose inner products yield

$$\begin{aligned}\langle \phi_A e^{i\omega_A t}, -\beta\mathbf{K}_{ee}\mathbf{x}^{(0)}_{e_t}\rangle &= -\,i\beta\omega_A^3 A,\\ \langle \phi_B e^{i\omega_B t}, -\beta\mathbf{K}_{ee}\mathbf{x}^{(0)}_{e_t}\rangle &= -\,i\beta\omega_B^3 B,\end{aligned} \tag{40}$$

since $\phi_A^\top\mathbf{K}_{ee} = \omega_A^2\phi_A^\top\mathbf{M}_{ee}$ and $\phi_B^\top\mathbf{K}_{ee} = \omega_B^2\phi_B^\top\mathbf{M}_{ee}$. Finally, projecting the forcing terms gives

$$\begin{aligned}&\langle \phi_A e^{i\omega_A t}, \frac{\mathbf{f}_A}{2}e^{i(\omega_A t+\Delta\omega_A\tau)} + \frac{\mathbf{f}_B}{2}e^{i(\omega_B t+\Delta\omega_B\tau)}\rangle =\\ &\frac{\phi_A^\top\mathbf{f}_A}{2}e^{i\Delta\omega_A\tau},\\ &\langle \phi_B e^{i\omega_B t}, \frac{\mathbf{f}_A}{2}e^{i(\omega_A t+\Delta\omega_A\tau)} + \frac{\mathbf{f}_B}{2}e^{i(\omega_B t+\Delta\omega_B\tau)}\rangle =\\ &\frac{\phi_B^\top\mathbf{f}_B}{2}e^{i\Delta\omega_B\tau}.\end{aligned} \tag{41}$$

Collecting Eqs. (37), (38), (40), and (41), we obtain the amplitude equations (18) and (19).

Author Contributions Javier González-Monge: Methodology, Investigation, Formal Analysis, Software, Visualization, Writing - Original Draft, Writing - Review & Editing. Salvador Rodríguez-Blanco: Methodology, Investigation, Formal Analysis, Software, Writing-Original Draft, Writing-Review & Editing. Carlos Martel: Methodology, Investigation, Formal Analysis, Supervision, Writing-Original Draft, Writing-Review & Editing.

Funding Open Access funding provided thanks to the CRUE-CSIC agreement with Springer Nature. The work of Javier González-Monge has been supported by Programa Propio de I+D+i de la Universidad Politécnica de Madrid.

Data Availability No datasets were generated or analysed during the current study.

Declarations

Conflicts of interest The authors declare that they have no conflict of interest.

References

1. Allgower, E.L., Georg, K.: Numerical continuation methods: an introduction, vol. 13. Springer Science & Business Media (2012). https://doi.org/10.1007/978-3-642-61257-2
2. Balaji, N.N., Gross, J., Krack, M.: Harmonic balance for quasi-periodic vibrations under nonlinear hysteresis. J. Sound Vib. **590**, 118570 (2024). https://doi.org/10.1016/j.jsv.2024.118570
3. Bender, C.M., Orszag, S.A.: Advanced mathematical methods for scientists and engineers I: Asymptotic methods and perturbation theory. Springer Science & Business Media (2013). https://doi.org/10.1007/978-1-4757-3069-2
4. Bladh, R., Castanier, M.P., Pierre, C.: Component-mode-based reduced order modeling techniques for mistuned bladed disks-part i: Theoretical models. J. Eng. Gas Turbines Power **123**(1), 89–99 (2000). https://doi.org/10.1115/1.1338947
5. Cameron, T.M., Griffin, J.H.: An alternating frequency/time domain method for calculating the steady-state response of nonlinear dynamic systems. J. Appl. Mech. **56**(1), 149–154 (1989). https://doi.org/10.1115/1.3176036
6. Craig, R.R., Jr., Bampton, M.C.: Coupling of substructures for dynamic analyses. AIAA J. **6**(7), 1313–1319 (1968). https://doi.org/10.2514/3.4741
7. Fontanela, F., Grolet, A., Salles, L., Hoffmann, N.: Computation of quasi-periodic localised vibrations in nonlinear cyclic and symmetric structures using harmonic balance methods. J. Sound Vib. **438**, 54–65 (2019). https://doi.org/10.1016/j.jsv.2018.09.002
8. González-Monge, J., Rodríguez-Blanco, S., Martel, C.: Friction-induced traveling wave coupling in tuned bladed-disks. Nonlinear Dyn. **106**(4), 2963–2973 (2021). https://doi.org/10.1007/s11071-021-06930-1
9. González-Monge, J., Rodríguez-Blanco, S., Martel, C.: Nonlinear switching between flutter and forced response in bladed disks. Nonlinear Dyn. **111**(6), 5237–5247 (2023). https://doi.org/10.1007/s11071-022-08140-9
10. González-Monge, J.: Nonlinear vibrations in turbomachinery: an asymptotic approach (2025). https://doi.org/10.20868/UPM.thesis.89915
11. Guillot, L., Vigué, P., Vergez, C., Cochelin, B.: Continuation of quasi-periodic solutions with two-frequency harmonic balance method. J. Sound Vib. **394**, 434–450 (2017). https://doi.org/10.1016/j.jsv.2016.12.013
12. Guskov, M., Thouverez, F.: Harmonic balance-based approach for quasi-periodic motions and stability analysis. J. Vib. Acoust. **134**(3), 031003 (2012). https://doi.org/10.1115/1.4005823
13. Krack, M., Gross, J.: Harmonic balance for nonlinear vibration problems, vol. 1. Springer (2019). https://doi.org/10.1007/978-3-030-14023-6
14. Krack, M., Salles, L., Thouverez, F.: Vibration prediction of bladed disks coupled by friction joints. Archives of Computational Methods in Engineering **24**, 589–636 (2017). https://doi.org/10.1007/s11831-016-9183-2
15. Martel, C., Corral, R.: Flutter amplitude saturation by nonlinear friction forces: An asymptotic approach. p. V07BT33A001 (2013). https://doi.org/10.1115/GT2013-94068
16. Martel, C., Corral, R., Ivaturi, R.: Flutter amplitude saturation by nonlinear friction forces: Reduced model verification. J. Turbomach. **137**(4), 041004 (2014). https://doi.org/10.1115/1.4028443
17. Menq, C., Yang, B.: Non-linear spring resistance and friction damping of frictional constraint having two-dimensional motion. J. Sound Vib. **217**(1), 127–143 (1998). https://doi.org/10.1006/jsvi.1998.1739
18. Olofsson, U.: Cyclic micro-slip under unlubricated conditions. Tribol. Int. **28**(4), 207–217 (1995). https://doi.org/10.1016/0301-679X(94)00001-7
19. Petrov, E., Ewins, D.: State-of-the-art dynamic analysis for non-linear gas turbine structures. Proceedings of the Institution of Mechanical Engineers, Part G: Journal of Aerospace Engineering **218**(3), 199–211 (2004). https://doi.org/10.1243/0954410041872906
20. Petrov, E.P.: Analysis of bifurcations in multiharmonic analysis of nonlinear forced vibrations of gas turbine engine structures with friction and gaps. J. Eng. Gas Turbines Power **138**(10), 102502 (2016). https://doi.org/10.1115/1.4032906
21. Petrov, E.P., Ewins, D.J.: Analytical formulation of friction interface elements for analysis of nonlinear multi-harmonic vibrations of bladed disks. J. Turbomach. **125**(2), 364–371 (2003). https://doi.org/10.1115/1.1539868
22. Rodríguez, S., Martel, C.: Analysis of experimental results of turbomachinery flutter using an asymptotic reduced order model. J. Sound Vib. **509**, 116225 (2021). https://doi.org/10.1016/j.jsv.2021.116225
23. Rodríguez-Blanco, S., González-Monge, J., Martel, C.: Asymptotic evaluation of nonlinear friction effects in realistic lpt rotors. p. V11BT27A017 (2023). https://doi.org/10.1115/GT2023-102829
24. Sanliturk, K.Y., Imregun, M., Ewins, D.J.: Harmonic balance vibration analysis of turbine blades with friction dampers. J. Vib. Acoust. **119**(1), 96–103 (1997). https://doi.org/10.1115/1.2889693
25. Sarrouy, E., Sinou, J.J.: Non-linear periodic and quasi-periodic vibrations in mechanical systems-on the use of the harmonic balance methods. Advances in vibration analysis research **21**, 419 (2011). https://doi.org/10.5772/15638
26. Schwingshackl, C., Petrov, E., Ewins, D.: Measured and estimated friction interface parameters in a nonlinear dynamic analysis. Mechanical Systems and Signal Processing **28**, 574–584 (2012). https://doi.org/10.1016/j.ymssp.2011.10.005. Interdisciplinary and Integration Aspects in Structural Health Monitoring
27. Zhou, B., Thouverez, F., Lenoir, D.: A variable-coefficient harmonic balance method for the prediction of quasi-periodic response in nonlinear systems. Mech. Syst. Signal Process. **64–65**, 233–244 (2015). https://doi.org/10.1016/j.ymssp.2015.04.022
28. Zucca, S., Firrone, C.M., Gola, M.M.: Numerical assessment of friction damping at turbine blade root joints by simultaneous calculation of the static and dynamic contact loads. Nonlinear Dyn. **67**, 1943–1955 (2012). https://doi.org/10.1007/s11071-011-0119-y